European Journal of Immunology
Clinical·Basic·Translational

Tumor immunology

Clinical

Research Article

Dimethyl itaconate selectively targets inflammatory and metabolic pathways in chronic lymphocytic leukemia

Ilenia Sana[1], Maria Elena Mantione[1], Miriam Meloni[1], Michela Riba[2], Pamela Ranghetti[3], Lydia Scarfò[3,4], Paolo Ghia[3,4] and Marta Muzio[1]

[1] Cell signaling Unit, Division of Experimental Oncology, IRCCS San Raffaele Scientific Institute, Milano, Italy
[2] Center for Omics Sciences, IRCCS San Raffaele Scientific Institute, Milano, Italy
[3] B-cell neoplasia Unit, Division of Experimental Oncology, IRCCS San Raffaele Scientific Institute, Milano, Italy
[4] Vita-Salute San Raffaele University, Milano, Italy

Chronic lymphocytic leukemia (CLL) co-evolves with its own microenvironment where inflammatory stimuli including toll-like receptors (TLR) signaling can protect CLL cells from spontaneous and drug-induced apoptosis by upregulating IκBζ, an atypical co-transcription factor. To dissect IκBζ-centered signaling pathways, we performed a gene expression profile of primary leukemic cells expressing either high or low levels of IκBζ after stimulation, highlighting that IκBζ is not only an inflammatory gene but it may control metabolic rewiring of malignant cells thus pointing to a novel potential opportunity for therapy. We exploited the capacity of the dimethyl itaconate (DI), an anti-inflammatory electrophilic synthetic derivative of the metabolite Itaconate, to target IκBζ. CLL cells, murine leukemic splenocytes, and leukocytes from healthy donors were treated *in vitro* with DI that abolished metabolic activation and reduced cell viability of leukemic cells only, even in the presence of robust TLR prestimulation. RNA sequencing highlighted that in addition to the expected electrophilic stress signature observed after DI treatment, novel pathways emerged including the downregulation of distinct MHC class II complex genes. In conclusion, DI not only abrogated the proinflammatory effects of TLR stimulation but also targeted a specific metabolic vulnerability in CLL cells.

Keywords: B cells · Chronic lymphocytic leukemia · Dimethyl Itaconate · Inflammation · Toll like receptors

Additional supporting information may be found online in the Supporting Information section at the end of the article.

Introduction

Chronic lymphocytic leukemia (CLL), the most common malignancy of mature B cells, has a very heterogeneous clinical course in which the extrinsic component of the tumor plays a fundamental role in driving the progression and fate of leukemic cells. CLL cells maintain the expression of their unique B-cell receptor indispensable to receive survival signals as shown by the impressive clinical efficacy of novel kinase inhibitors [1]. Despite these advancements, profound responses are obtained only in a minority of patients and relapses still occur rendering it crucial to identify and target accessory and/or compensatory signals

Correspondence: Dr. Marta Muzio
e-mail: muzio.marta@hsr.it

from the surrounding microenvironment including inflammatory stimuli [2]. A recent paper revealed resistance mechanisms operating in different and/or novel prognostic subgroups of CLL pointing again on cytokines (IL4) and TLR ligands (TLR7 and TLR9) as the strongest actuators of drug resistance [3]. Moreover, TLR-mediated signaling in LN-resident CLL cells is only partially inhibited by BTK inhibitory drugs [2] raising the urgent need for the identification and targeting of novel molecular circuits.

Relevant to mention is TLR9 signaling as this stimulation induces proliferation and migration of the leukemic clone in some CLL samples but promotes cell death in others [4–10]; to note, IκBζ was identified as one of the key molecules that endorses the survival of CLL cells. Specifically, the stimulation of TLR9 *in vitro* results in cell proliferation, metabolic activation, and protection from apoptosis mainly in patients' samples overexpressing IκBζ and bearing adverse prognostic markers [4, 10, 11]. IκBζ, an atypical member of the IκB family, is upregulated by STATs and NF-κB after IL1R and TLRs stimulation and regulates at chromatin level the expression of several inflammatory cytokines such as IL6 and IL10 [12]. In CLL cells, it can be induced at higher levels as compared with normal B-lymphocytes suggesting that targeting this transcriptional regulator may uncover a novel vulnerability in CLL [11]. However, it is unknown if and which different transcriptional programs are activated by IκBζ and if we could target them for therapeutic purposes.

To address these questions, we first performed a transcriptomic analysis of primary CLL samples under TLR9 stimulation to identify the pathways that are specifically related to high levels of IκBζ. Next, we focused on an inhibitory agent acting on IκBζ to test its therapeutic activity *in vitro* in different preclinical models of CLL.

Results

Transcriptional profiles of IκBζ-high versus IκBζ-low CLL samples

To analyze the IκBζ-linked transcriptional alterations in CLL cells, we performed RNAseq of primary leukemic cells purified from peripheral blood (PB) of patients and stimulated with CpG; we compared the response of IκBζ-high cases (IκBζ+ cells after 24 h CpG stimulation>29.75% respect to unstimulated sample, as we previously described) to the one observed in IκBζ low samples that are characterized by a TLR9 activation profile likely independent of IκBζ. Specifically, 4 IκBζ-High cases and 3 IκBζ-Low cases were either incubated *in vitro* for 4 h or treated with CpG. In the IκBζ-high cases, the stimulation altered the expression of 830 genes (Fig. 1A, left) while in the IκBζ-low cases, 126 genes were differentially expressed (Fig. 1A, right).

To understand which functions and processes are associated with TLR9-induced IκBζ expression, we compared transcriptomic profiles taking advantage of Metascape, a web-based platform that allows to compare multiple lists of genes [13]. As illustrated in Fig. 1B, inflammatory-related pathways were enriched through all CLL samples analyzed independent from IκBζ levels (e.g. GO inflammatory response). That notwithstanding, there was a strong enrichment of several RNA metabolic processes in IκBζ-High cases only, as well as stress responses (Fig. 1B).

To dissect which metabolic pathways are involved, we took advantage of OmicsNet, a web-based resource that analyzes specifically metabolic networks [14].

Analyzing the 552 genes upregulated in IκBζ-High samples, we observed an enrichment in one-carbon (1C) metabolism (n.Hits = 94; adj.*p* value = 1e-031) and a related increase in Purine metabolisms (Fig. 1C).

Overall, transcriptional analysis suggested that the prosurvival activity of IκBζ and increased ATP levels are related to a broad metabolic rewiring involving also 1C metabolism whose implication in cancer is well known [15]. We hypothesized that targeting IκBζ may at the same time interrupt the metabolic advantages of CLL cells.

Dimethyl itaconate treatment reduces IκBζ expression in CLL cells

Dimethyl itaconate (DI) is a synthetic derivative of TCA cycle secondary metabolite Itaconate with electrophilic properties that downmodulates an inflammatory axis centered on IκBζ [16, 17]. With respect to itaconate, DI has a lower negative charge due to esterification and increased capacity to cross the cell membrane; this modification impacts the electrophilicity of DI that may regulate additional pathways as compared with endogenous itaconate [16–18]. On this ground, we hypothesized that using the electrophilic compound DI, we may target the IκBζ inflammatory and metabolic axis thus increasing the therapeutic selectivity and specificity against CLL cells.

To partially mimic the TLR-stimulated nodal niche, we treated primary human leukemic cells with the TLR9 ligand CpG before (or after) drug treatment *in vitro*. We added DI to primary leukemic cells isolated from the PB of patients with CLL and, after different time points, we measured both the mRNA and protein levels with or without TLR9 stimulation with CpG. Specifically, we tested two different conditions: (A) PRE-CpG where CLL cells were cultured in the presence of DI overnight (ON) followed by CpG stimulation; (B) POST-CpG where CLL cells were incubated for 4 h with CpG and following treated with DI; the concentrations of DI were the same previously used in macrophages [16] (Fig. 2A and B). With the PRE-CpG and POST-CpG schedules, we would like to recapitulate both preventive and curative approaches.

To evaluate the effects of DI on IκBζ induction, we analyzed both protein and RNA expression with flow cytometry and qPCR analyses. As expected, IκBζ protein levels are heterogeneously increased by CpG among different CLL samples, confirming the presence of both "IκBζ-high" and "IκBζ-low" cases as previously described [11]. On the other hand, increasing concentrations of DI blocked IκBζ induction when cells were pretreated (Fig. 2C; $n = 11$, mean 50 μM = 16.96%, 100 μM = 7.7%, 200 μM =

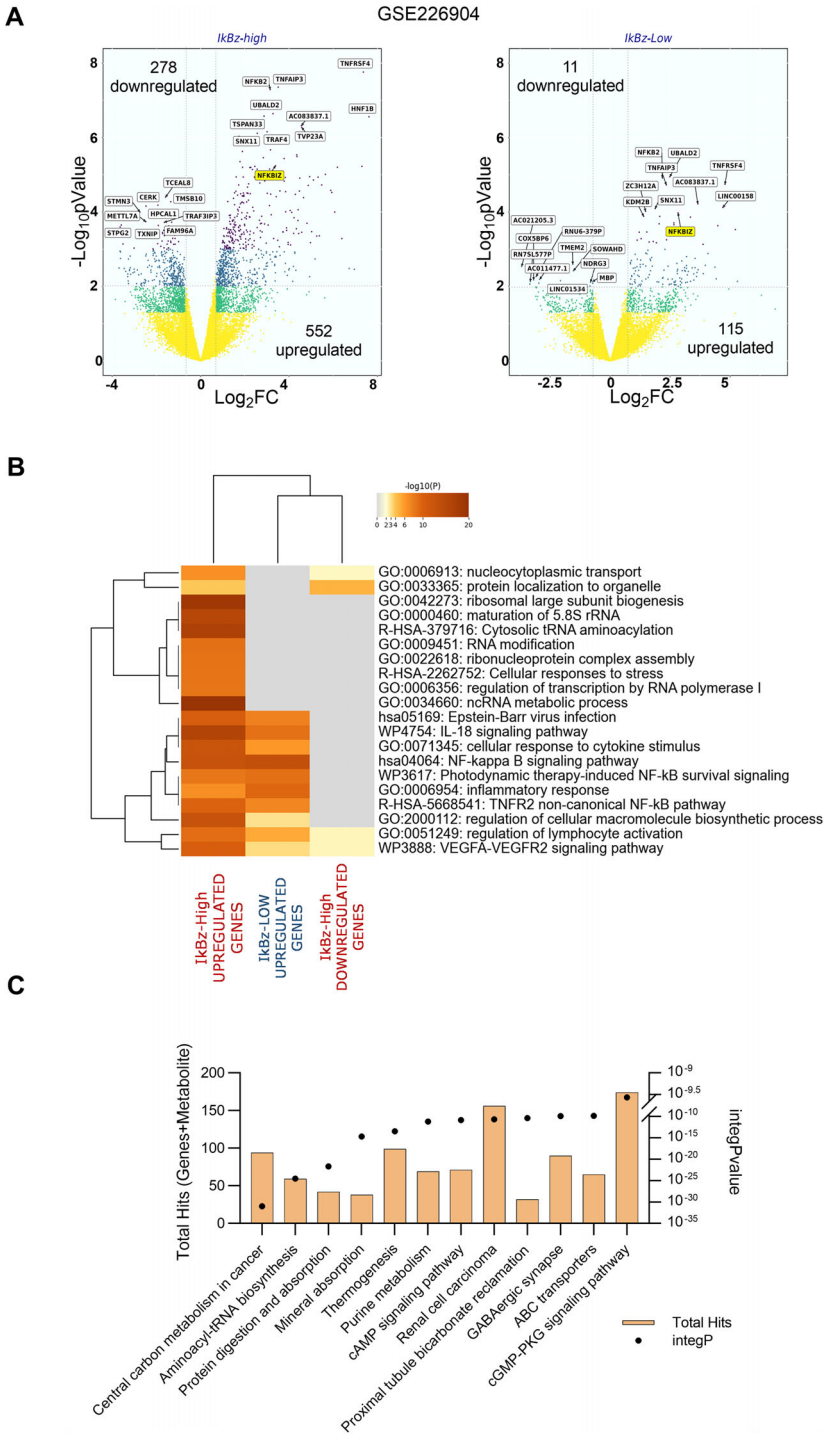

Figure 1. TLR9-mediated IκBζ induction and signaling pathways in CLL cells. (A) Volcano plots representing the overall response of $n = 4$ IκBζ-high donors (left) and $n = 3$ IκBζ-low donors (right) to 4 h of CpG stimulation. CLL cells were isolated from peripheral blood of patients and cultured for 4 h in the presence or the absence of CpG 2.5 μg/mL. Total RNA was extracted and sequencing was performed. Volcano plots were generated using Log_2FC and p value of stimulated samples RNA profiles versus their unstimulated counterparts. Differentially expressed genes were determined with SEQC method: p value < 0.01 & $|\log_2 fc| > 1$. (B) Enrichment analysis of the lists of DEGs was performed with Metascape [13]; the Heatmap shows the top 20 enriched terms among the lists of DEGs. (C) Metabolic enrichment analysis was performed with OmicsNet with list of upregulated genes in IκBζ-high profiles. KEGG-based metabolic network was constructed and then enrichment analysis was performed on the reconstructed network of genes and related metabolite.

3.3%). Increasing doses of DI were effective also in the POST-CpG setting (Fig. 2D; $n = 10$).

Focusing on mRNA induction, 4 hours of TLR9 activation induced a 12-fold change (FC) increase of *NFKBIZ* mRNA while in the PRE-treated samples (green bar) DI significantly repressed *NFKBIZ* mRNA induction to three-fold. In the POST setting (blue bar), DI-treated samples showed a trend of decrease compared with CpG-stimulated ones (Fig. 2E).

Finally, we tested the functional effects of the DI-mediated inhibition by analyzing two known target genes, namely IL6 and IL10. As shown in Fig. 2F, *IL6* induction was significantly blocked when DI was added before TLR9 stimulation, and a trend of reduction was observed when DI was added after CpG. Similarly, *IL10* mRNA levels were 23.16 FC in the CpG stimulated samples over the untreated, and 12.23 and 3.38 in the PRE- and POST-settings, respectively, though the decrease was highly variable and not statistically significant (Fig. 2G).

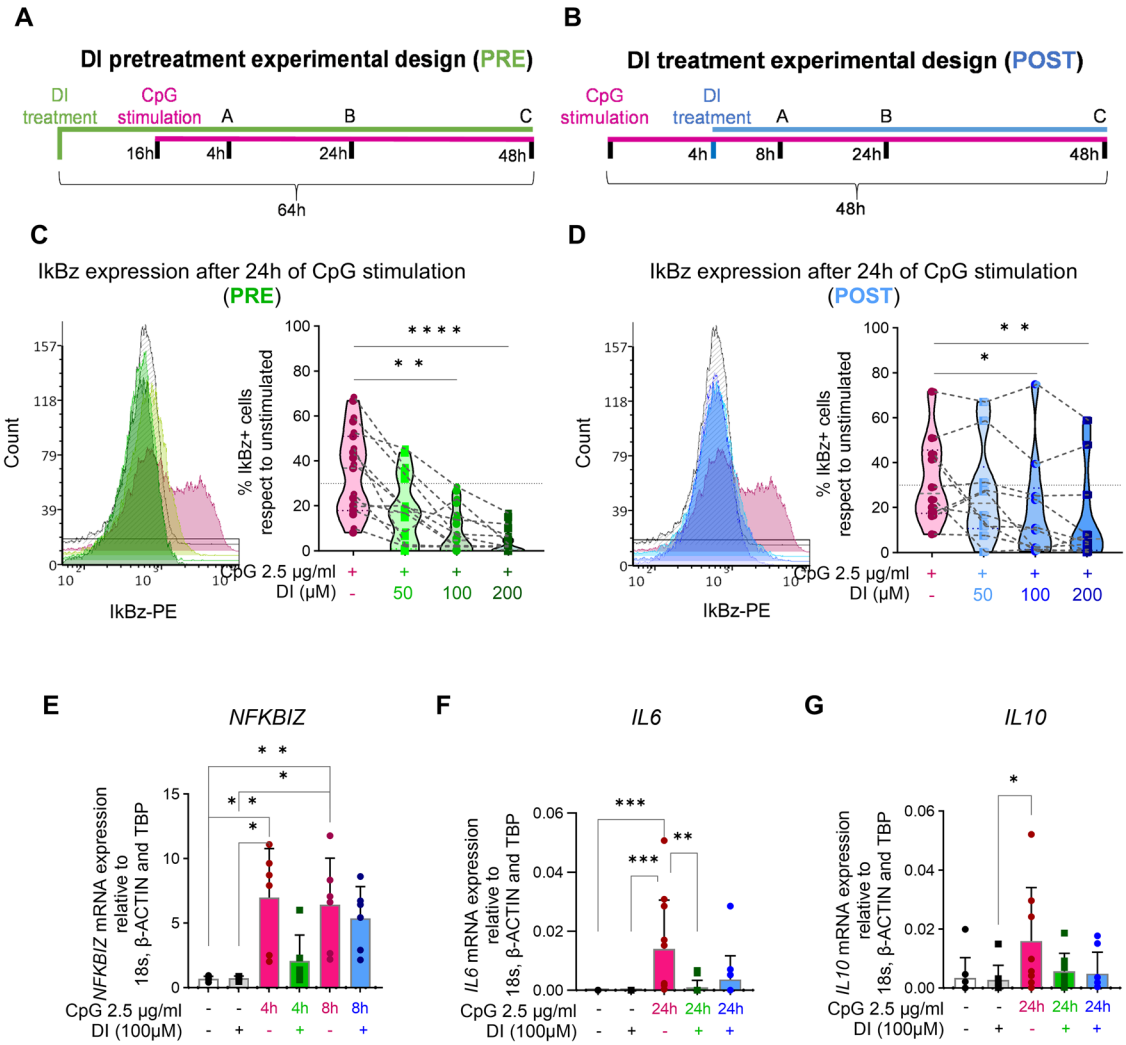

Figure 2. Dimethyl itaconate (DI) abrogates TLR9-mediated IκBζ induction in CLL cells. Schematic representation of PRE-CpG (A) and POST-CpG (B) schedule. In both experimental procedures, *NFKBIZ* RNA was quantified at time point "A". At time point "B", Western blot and flow cytometry analysis was performed. At time point B and C, metabolic activation and cell viability were quantified. For RNA-seq analysis RNA was extracted at time point "A" only in the PRE-CPG Schedule. We tested both the PRE-CpG (green) and POST-CpG (blue) schedules to specifically evaluate the effects of increasing doses of DI (50-200 μM) on ATP levels and viability of purified CLL cells. IκBζ quantification by flow cytometry in primary CLL cells stimulated for 24 h with CpG in the presence of increasing concentration of DI following the PRE (C) and POST (D) schedule (n = 11 independent experiments in PRE; n = 10 independent experiments in POST). One representative sample is shown in left panel for PRE and POST respectively. (E) *NFKBIZ* mRNA quantification relative to *18s*, *β-actin*, and *TBP* after 4/8 h of CpG stimulation in the presence or not of 100 μM of DI (n = 6 independent experiment). (F–G) *IL6* (n = 13 samples in 11 independent experiments) and *IL10* (n = 8 samples in five independent experiments) mRNA quantification relative to *18s*, *β-actin*, and *TBP* after 24 h of CpG stimulation in the presence or not of 100 μM of DI. One-way ANOVA analyses were performed, and Turkey or Dunn posttests were done for multiple *comparisons*. *$p < 0.05$; **$p < 0.01$; ***$p < 0.001$; ****$p < 0.0001$.

In conclusion, the addition of DI before CpG stimulation and to a lesser extent after CpG stimulation blocked both *NFKBIZ* mRNA and protein as well as its target genes.

DI blocks metabolic activation of leukemic cells and induces apoptosis

To test the efficacy of DI to inhibit TLR-induced IκBζ-mediated metabolic activation, we quantified the ATP present in purified CLL cells cultured *in vitro*. As expected, CpG treatment induced a heterogeneous increase of ATP production at both 24 (Fig. S1A) and 48 hours as compared with untreated samples (48 h CpG = 125%, SD = 40.45, n = 15, p = 0.0353; Fig. 3A); on the other hand, increasing concentrations of DI pretreatment significantly reduced the energy production induced by TLR9 stimulation. We then asked if DI could inhibit metabolic activation and promote cell death when added after the stimulation of TLR9 and consequent high expression of IκBζ as this would more closely mimic the *in vivo* situation where ongoing TLR signaling was reported in the lymph nodes [2]. Even in this most stringent experimental setting (POST-CpG), a dose-dependent reduction of the cellular

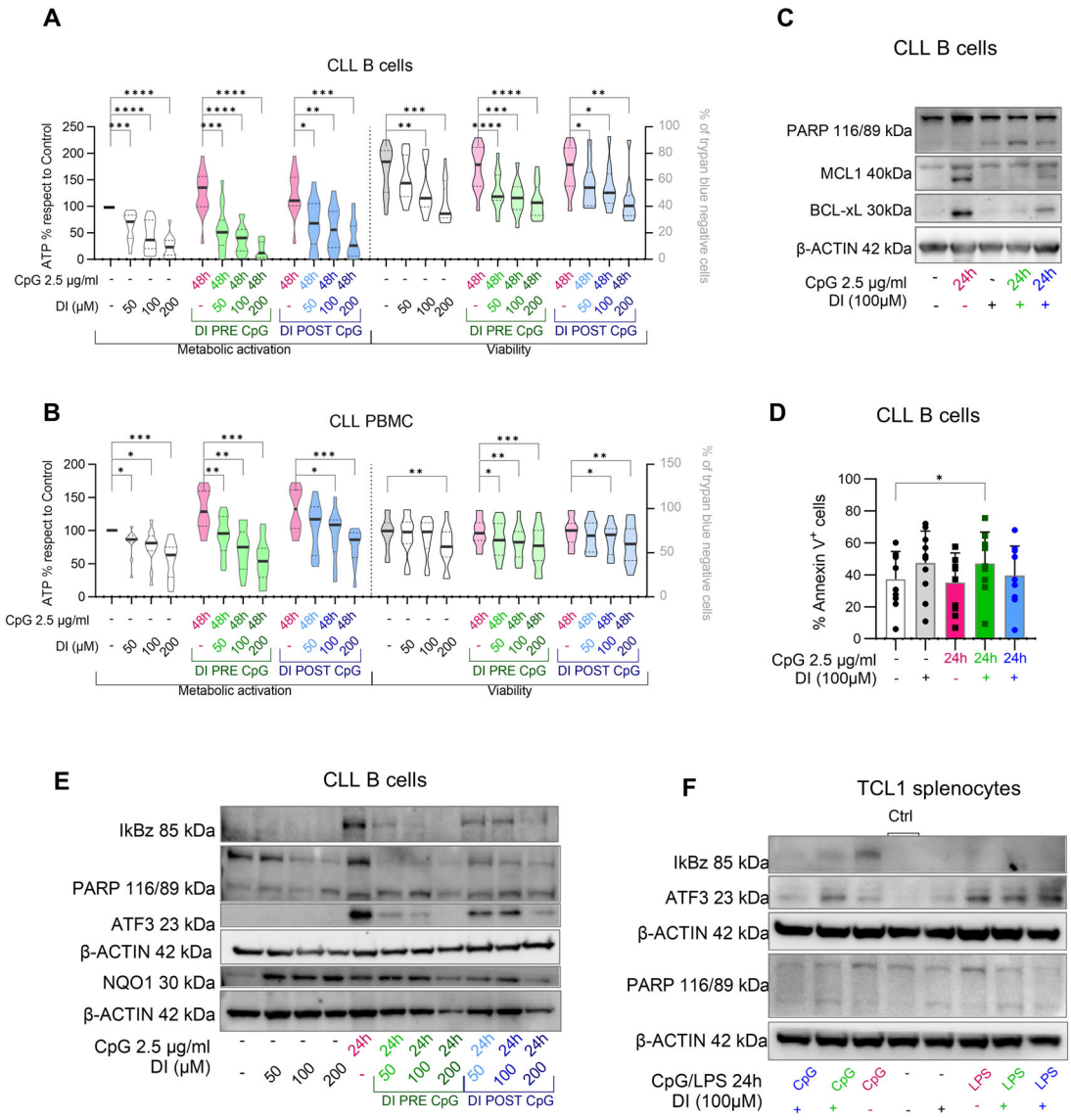

Figure 3. DI selectively reduces metabolic activation and survival of primary CLL cells, sparing healthy leukocytes. We tested both the PRE-CpG (green) and POST-CpG (blue) schedules to specifically evaluate the effects of increasing doses of DI (50-200µM) on ATP levels and viability of purified CLL cells (A) PBMC from CLL patients (B), in the presence or not of TLR9 stimulation. Using cell titer Glo assay, after 48 h of TLR9 stimulation (2.5 µg/mL CpG) we quantified the percentage of ATP present in the cells with respect to the Ctrl samples as a measure of their metabolic activation (A left $n = 15$ samples in nine independent experiments), B left $n = 12$ samples in 10 independent experiments). Using TC20 automated cell counter we measured the percentage of viable trypan blue negative cells after 48 h of TLR stimulation (2.5 µg/mL CpG) (A right $n = 13$ samples in nine independent experiments), B right n = 11 samples in eight independent experiments). Two-way ANOVA analysis was performed and Dunnet posttest was performed for multiple comparisons. $^{*}p < 0.05$; $^{**}p < 0.01$; $^{***}p < 0.001$; $^{****}p < 0.0001$. (C) Western blot analysis of one representative CLL sample treated with 100 µM DI in the presence or not of CpG for 24 h (in green PRE-CpG setting, in blue POST-CpG setting). PARP, BCL-xL, and MCL1 expression were evaluated. (D) Using Flow Cytometry we measured the percentage of Annexin V positive cells in CLL cells PRE-treated ON or POST-treated with 100 µM DI after 24 h of CpG stimulation ($n = 10$ samples in six independent experiments). One-way ANOVA analysis was performed and Dunnet posttest was performed for multiple comparisons. $^{*}p < 0.05$; $^{**}p < 0.01$; $^{***}p < 0.001$; $^{****}p < 0.0001$. (E) Western blot analysis of one representative (out of 3) CLL sample treated with increasing concentration of DI in the presence or not of CpG for 24 h (50 µM–100 µM–200 µM; in green PRE-CpG setting, in blue POST-CpG setting). (F) Western blot analysis of one (out of 3) representative sample of leukemic TCL1-tg mice-derived splenocytes stimulated 24 h with 2.5 µg/mL CpG-ODN1826 (murine specific) or 1 µg/mL LPS in the presence or not of 100 µM of DI (green = PRE; blue = POST).

metabolic state is evident as compared with untreated samples; specifically, the percentage of ATP levels dropped to 37.23% ± 35 at the maximal dose of DI as compared with untreated control (Fig. 3A).

Since the intracellular levels of ATP reflect both metabolic state and cell viability, we monitored the percentage of trypan blue positive versus negative cells under the same experimental conditions using an automated cell counter (Fig. 3A, 48 h; Fig. S1A, 24 h); as expected, after 48 h of *in vitro* culture untreated leukemic cells started to dye (67.98% ± 17.88 cell viability) and DI treatment decreased the percentage of viable cells to 60.87% ± 16.92 at 50 µM, 52.07% ± 18.19 at 100 µM DI, and 43.12% ± 15.9 at

200 μM DI ($n = 12$ samples for all the doses). DI PRE-treatment induced cell death even in the presence of CpG. Notably, DI was effective even when added after TLR9 stimulation (Fig. 3A). Overall, we observed a dose-dependent reduction in cell viability at both 24 and 48 h, with or without CpG stimulation that reflected, at lower levels, the impact on metabolic activation.

To address the activity of DI on cells expressing different amounts of IκBζ, we divided our small cohort of samples into IκBζ-high versus IκBζ-low (cut off 29.75% positive cells 24 h after CpG stimulation as previously reported) [11] and we re-analyzed both cell activation and cell viability after 100 μM DI treatment ($n = 36$; IκBζ-high $n = 18$; IκBζ-low $n = 18$;). As reported in Fig. S2, DI reduced cell viability in both IκBζ-low and IκBζ-high samples. Moreover, DI reverted the increased CpG-mediated cellular activation which is more evident in IκBζ-high samples where DI reduced the ATP content of CpG-treated cells from 141% to 40%; in IκBζ-low samples, the CpG effect was less evident (107% respect to control) and was inhibited by DI as well (37%). Overall, these data suggest that the impact of DI is associated only partially with the expression levels of IκBζ. However, DI was very effective in abrogating the cytoprotective effects of CpG that are found mainly in IκBζ-high samples.

Next, we tested the effect of DI on PBMC isolated from the blood of patients with CLL ($n = 12$) because the non-leukemic cellular fractions have a protective effect against drug treatment [19]. To note, even under these experimental conditions, DI not only blocked the effects of CpG on metabolic activation but also induced cell death with or without TLR9 stimulation, in both PRE- and POST-setting (Fig. 3B, 48 h; Fig. S1B, 24 h).

To further validate our results in a different preclinical model of CLL, we tested DI *ex vivo* on leukemic cells collected from TCL1 transgenic mice and treated with LPS obtaining similar results (Fig. S3) [20].

To identify the type of DI-induced cell death, we quantified the percentage of Annexin V positive cells (Fig. 3D), we analyzed the expression of BCL-xL, MCL1, and PARP1 (Fig. 3C), and we quantified the cleavage of PARP1 after densitometric analysis in primary CLL cells (Fig. S4A). DI promoted apoptosis either alone or in combination with CpG as demonstrated by the reduction of both MCL1 and BCL-xL, by the increased rate of PARP1 cleavage as compared with the total amount expressed and the increase in Annexin V positive cells (Fig. 3C). Similar results were obtained in murine leukemic cells where PARP1 was cleaved in DI-treated samples (Fig. 3F).

Normal peripheral blood mononuclear cells are resistant to DI treatment

To evaluate the effect of DI treatment on normal leukocytes which may result in potential toxicity, we treated peripheral blood mononuclear cells (PBMC) isolated from PB of healthy donors; briefly, we either pretreated the cells ON with DI (PRE-CpG schedule) or treated with DI 4 h after CpG stimulation (POST-CpG). 24 and 48 h after CpG stimulation, we measured the ATP levels and the percentage of viable trypan blue negative cells. TLR9 triggering did not affect metabolic activation or cell viability of PBMC; both PRE-CpG and POST-CpG treatment with DI did not influence leukocytes survival (Fig. 4A, 48h; Fig. S1C, 24 h), and no significant toxic effect could be detected even at the highest dose of 200 μM DI.

These results suggest a leukemic or a B-cell-specific effect of DI. To analyze the impact of DI on different cell populations, we treated healthy PBMC with 100 μM of DI before or after CpG stimulation. We then stained the cells with a viability dye and analyzed by flow cytometry viable $CD5^+/CD19^-$ cells (i.e. T-lymphocytes), $CD5^-/CD19^+$ cells (i.e. B-lymphocytes), and $CD16^+$ cells (i.e. monocytes and NK cells). Mirroring the result in Fig. 4A, we did not observe any significant difference in the distribution of viable cells except for a trend of reduction of $CD5^+$ cells after CpG (Fig. 4C; $n = 8$). Focusing on the B-cell compartment, a trend toward a cytoprotective effect by CpG was observed while DI did not affect cell survival (Fig. 4D; green columns for $CD19^+$ cells; $n = 8$).

We performed a comparative study between primary CLL cells and nonmalignant B cells isolated from healthy donors. We evaluated their response after 4 and 24 h of CpG stimulation (Fig. 4E and F, respectively), in the presence or absence of DI; we included also nonmalignant PBMC isolated from healthy donors at 24 h (Fig. 4E). As expected, in nonmalignant B cells, after 24 h of TLR9 stimulation, the levels of IκBζ are comparable with those of IκBζ-low patients (Fig. 4F) [11]; in contrast, IκBζ was undetectable in nonmalignant PBMC (Fig. 4E). After 4 h of stimulation, nonmalignant B cells express lower levels of *NFKBIZ* mRNA and IκBζ protein than CLL cells (Fig. 4B and E, respectively). CLL cells are known to have constitutive activation of NF-κB p65, and IκBζ is a known interactor of NF-κB; for this reason, we analyzed phospho p65 in normal and leukemic B cells, and we confirmed higher phosphorylation levels in CLL cells and found lower responsiveness in healthy B cells (Fig. 4E and F). This *in vitro* analysis demonstrated that DI treatment targeted malignant cells strongly suggesting a rather specific antileukemic effect likely related to differential activation of the NF-κB pathway.

DI induces NQO1 but not ATF3

To explore the molecular pathways regulated by DI in leukemic cells we focused on ATF3, the key transcription factor regulating the effect of itaconate in murine macrophages where ATF3 was induced [16]. However, DI alone was unable to increase ATF3 protein in CLL cells. On the other hand, CpG-stimulated cells increased ATF3 protein, and when DI was added before CpG, a trend of reduction of ATF3 was observed though variable among patients (Fig. 3E). ATF3 induction by CpG and LPS in TCL1-tg splenocytes was less evident compared with human CLL cells, and DI treatment alone exerted a trend of induction only (Fig. 3F).

Next, we analyzed the NQO1 protein as a prototypic target of NRF2-mediated electrophilic stress previously shown to be

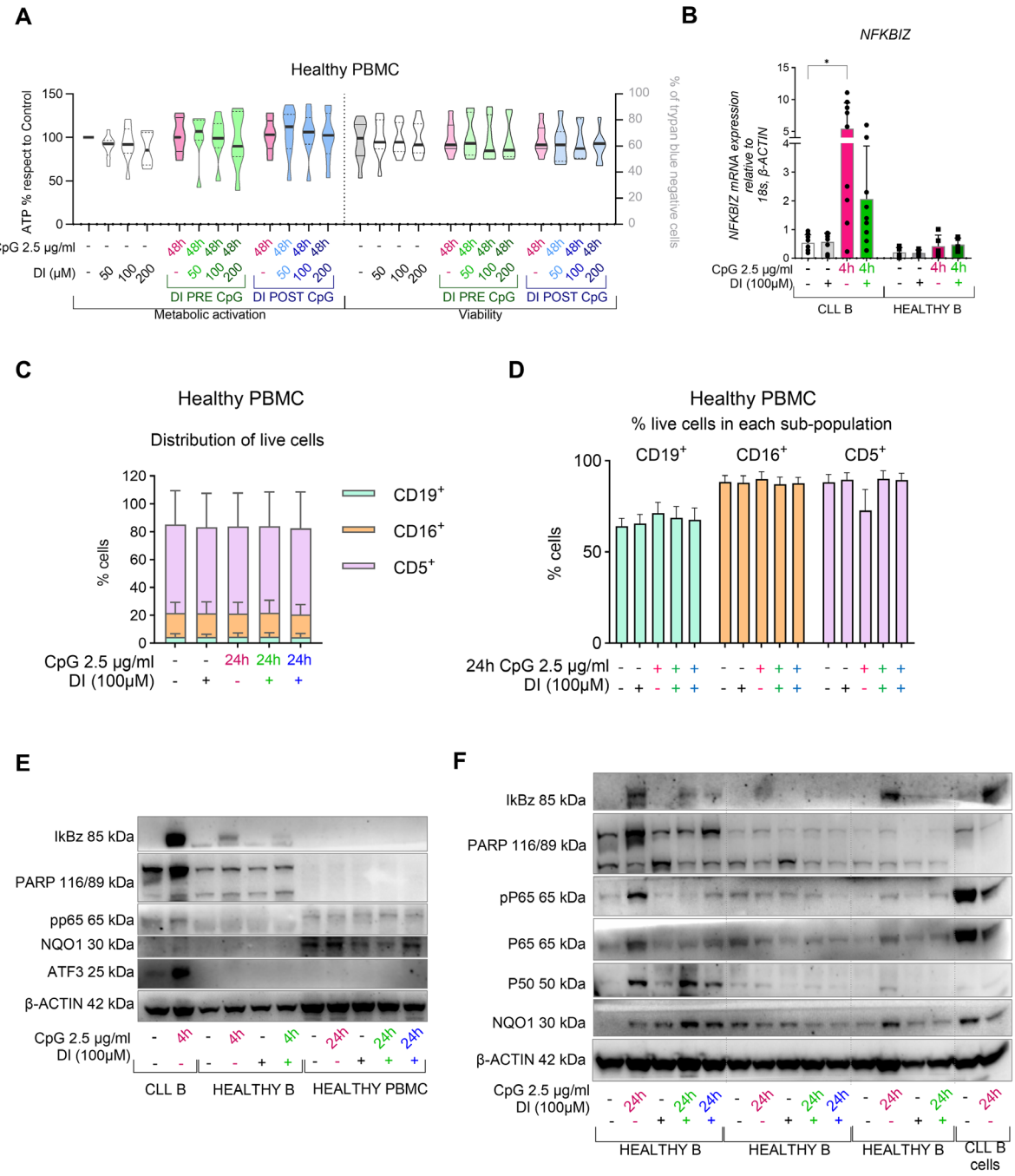

Figure 4. DI selectively reduces metabolic activation and survival of primary CLL cells. (A) We tested both the PRE-CpG (green) and POST-CpG (blue) schedules to specifically evaluate the effects of increasing doses of DI (50–200 μM) on ATP levels and viability of purified PBMC from healthy donors, in the presence or not of TLR9 stimulation. Using Cell titer Glo assay, after 48 h of TLR9 stimulation (2.5 μg/mL CpG) we quantified the percentage of ATP present in the cells with respect to the Ctrl samples as a measure of their metabolic activation (A left). Using TC20 automated cell counter we measured the percentage of viable trypan blue negative cells after 48 h of TLR9 stimulation (2.5 μg/mL CpG) (A right). $N = 8$ samples in four independent experiments. Two-way ANOVA analysis was performed and Dunnet posttest was performed for multiple comparisons. $^{*}p < 0.05$; $^{**}p < 0.01$; $^{***}p < 0.001$; $^{****}p < 0.0001$. (B) *NFKBIZ* mRNA quantification relative to *18s and β-actin* after 4 h of CpG stimulation in the presence or not of 100 μM of DI ($n = 9$ CLL cells in nine independent experiments; $n = 5$ nonmalignant B cells in three independent experiments). Two-way ANOVA analyses were performed, and Dunnet posttests were done for multiple *comparisons*. $^{*}p < 0.05$; $^{**}p < 0.01$; $^{***}p < 0.001$; $^{****}p < 0.0001$. (C, D) Using flow cytometry we measured the distribution (C) and the viability (D) of $CD5^{+}$, $CD16^{+}$, and $CD19^{+}$ populations of leukocytes in healthy PBMC PRE-treated ON or POST-treated with 100 μM DI after 24 h of CpG stimulation ($n = 8$ samples in seven independent experiments). Two-way ANOVA analysis was performed and Dunnet posttest was performed for multiple comparisons. $^{*}p < 0.05$; $^{**}p < 0.01$; $^{***}p < 0.001$; $^{****}p < 0.0001$. (E) Western blot analysis of one representative sample of CLL and purified B cells, total PBMC derived from healthy donors stimulated 4 h/24 h with CpG in the presence or not of 100 μM of DI (out of 3). (F) Western blot analysis of three representative samples of purified B cells from healthy donors stimulated 24 h with CpG in the presence or not of 100 μM of DI.

induced by DI in mouse macrophages. In the presence of DI, leukemic cells showed a trend of higher amounts of NQO1 mRNA (in five out of eight samples Fig. S4B) confirmed by western blot analysis (Fig. 3E and Fig. S4C for densitometric analysis of five samples).

Finally, we analyzed these same pathways also in PBMC and B-lymphocytes isolated from healthy donors; DI heterogeneously and slightly increases NQO1 in healthy PBMC cells where it is higher with respect to CLL cells (Fig. 4E and F). ATF3 expression is induced mainly in CpG-stimulated CLL cells (Fig. 4E) where it is inhibited by DI (Fig. 3E).

DI abrogates TLR signaling pathways and promotes NRF2-mediated stress response

To explore the molecular mechanism through which DI targets leukemic cells, we performed RNAseq analysis on primary CLL cells treated with 100 μM of DI, in the presence or absence of 4 h of TLR9 stimulation.

DI, either alone or with CpG, perturbed 276 common genes suggesting a DI-specific pathway alteration (e.g. TXN, HSPA1L/HSP70, HSP90, HMOX1; Fig. 5 and Fig. S5). To note, among the top 50 differentially expressed genes (DEGs) HLA-DQA1, an MHC class II complex gene, was significantly downregulated by the presence of DI.

Moreover, DI abrogated CpG effects; TLR9 activation upregulated 433 genes and downregulated 216 genes of which only 55 and 41 remained differentially expressed with DI pretreatment (Fig. 5A and B; Fig. S5). Among the DI-regulated genes, we confirmed *NFKBIZ, IL6*, and *IL10* together with other inflammatory genes including cytokines and chemokines (Fig. 5B).

To analyze the transcriptomic profiles at a system level and to identify the pathways affected by the treatments, we performed an enrichment and protein–protein interaction (PPI) analysis with Metascape. Using the lists of DEGs, we compared both the upregulated and downregulated genes by the treatment alone or in combination with the stimulation (DI up, DI down, CpG up, CpG down, DI+CpG up, DI+CpG down). To highlight the TLR-activated pathways specifically abrogated by DI, we also extracted the lists of genes differentially expressed in the transcriptomic profiles of DI+CpG samples as compared with stimulated samples only (DI+CpG vs. CpG-up, DI+CpG vs. CpG-down). The PPI analysis of all these lists merged highlighted the presence of distinctive subnetworks specific to the different treatments (Fig. 5C). In detail, the pretreatment with DI abrogated the wave of inflammation promoted by TLR9 as witnessed by the cytokines signaling subnetwork (SN1) together with cyclin-dependent kinases (SN5) and the ribosomal RNA metabolic processes network (SN2; Fig. 5C and Fig. S6). DI alone promoted a stress-dependent alteration that is even boosted in the presence of CpG with three key subnetworks: NRF2 stress-related transcriptional activity protein folding and ubiquitination including *KEAP1, ATF3*, and heat shock proteins (SN3,4,8; Fig. 5C; Figs. S6, S7, S8, and S9). In addition, DI downregulated several genes grouped in the subnetwork specific for antigen processing and presentation (SN6; Fig. 5C; Figs. S6 and S8).

An enrichment analysis was performed and the top 20 enriched pathways among all the lists are shown in Fig. 6A; moreover, a specific analysis for transcription factors regulation was performed on DEGs as shown in Fig. 6B and confirmed that key inflammatory NF-κB family members activated by CpG are counteracted by DI. DI-specific transcription factors signature included ATF4 and HSF1 further reinforcing a stress-related response (Fig. 6A and B). To identify the genes involved in this perturbation, we re-analyzed the expression of the single genes and created a heat plot specific for these pathways (Fig. 6C). This analysis further confirmed that stress-related genes such as *NQO1, KEAP1*, and *HMOX1* are specifically induced by DI. Among them, several transcripts related to Heat shock proteins and factors emerged (Fig. 6C).

Discussion

The aim of this project was twofold: (1) to identify IκBζ-related transcriptional programs in primary CLL samples. (2) to target IκBζ in preclinical models of CLL.

The analysis of primary CLL samples identified a unique IκBζ-related transcriptomic profile where prototypic inflammatory genes were present though they represent marginal part of the gene expression pattern. Our results support the existence of transcriptional program that drives typical inflammatory molecules while at the same time rewiring the metabolic state of the malignant cells in IκBζ-High samples. Exploiting a synthetic derivative of the endogenous metabolite itaconate, we could target IκBζ whereas at the same time inducing metabolic stress leading to leukemic cell death.

To partially mimic the nodal niche, we used a reductionist approach by prestimulating primary human leukemic cells with the TLR9 ligand CpG before or after drug treatment *in vitro*. We incubated primary leukemic cells with DI because it was known to act as an IκBζ inhibitor in different models of inflammation [16]; moreover, DI is an electrophilic molecule, and this class of compounds was previously shown to be preferentially active on leukemic cells [21]. The use of DI is currently proposed as a novel putative treatment strategy for several inflammatory-mediated diseases including cardiovascular diseases where a recent report showed that DI-loaded nanofibers reduce inflammation and help to repair myocardic infarction [16, 22–25]. In the context of cancer, DI showed anticancer activity in mouse models of hepatocellular carcinoma [26] and protected mice from colitis-associated colorectal cancer through its anti-inflammatory effects [27]. A recent report demonstrated an antitumor effect of DI on a thymic carcinoma cell line [28]; however, our data show for the first time as proof of principle a direct therapeutic effect of DI on primary leukemic cells.

We observed a dose-dependent block of IκBζ induction by DI pretreatment, and a decrease when DI was added after CpG stimulation. DI treatment of leukemic cells reduced TLR-mediated

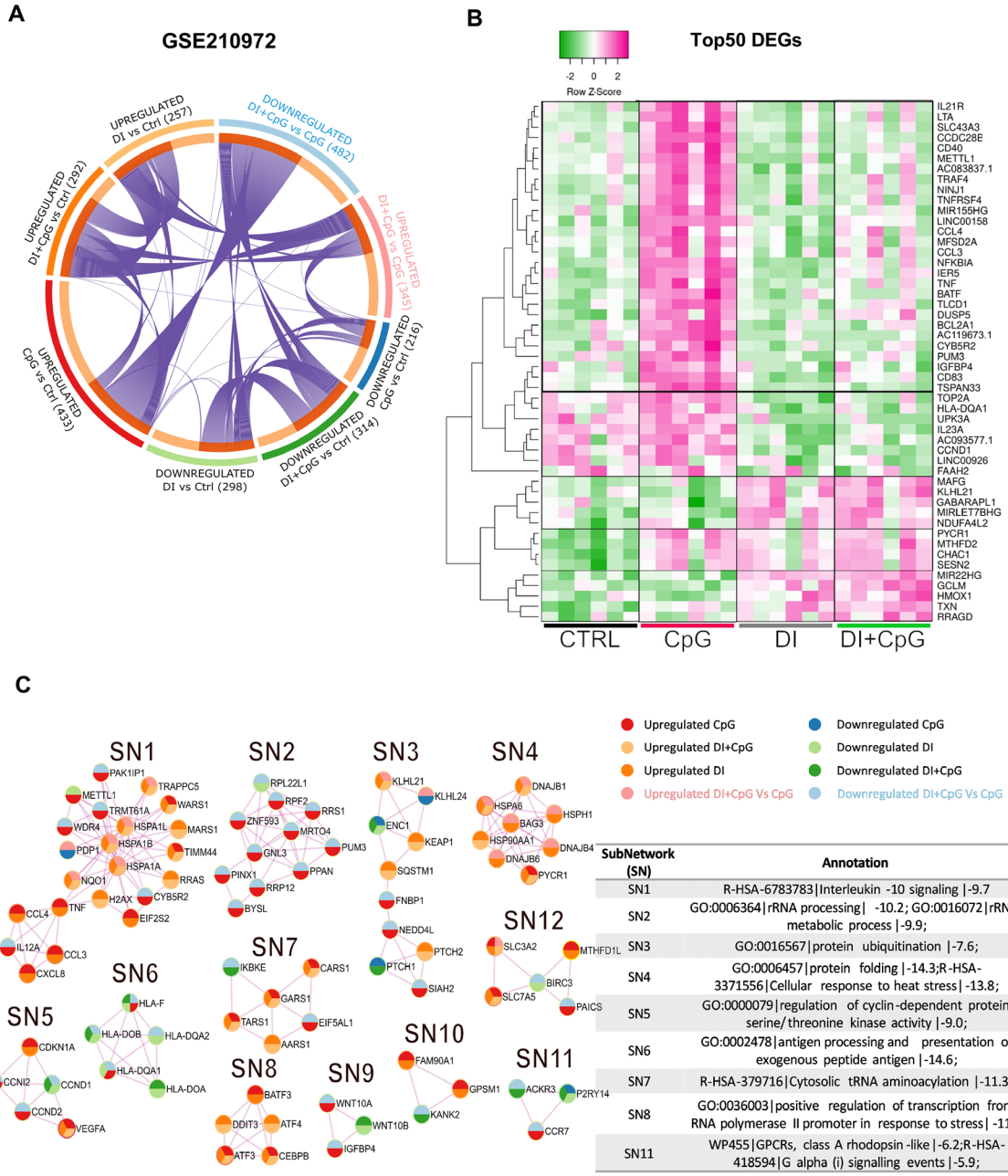

SubNetwork (SN)	Annotation
SN1	R-HSA-6783783|Interleukin -10 signaling |-9.7
SN2	GO:0006364|rRNA processing| -10.2; GO:0016072|rRNA metabolic process |-9.9;
SN3	GO:0016567|protein ubiquitination |-7.6;
SN4	GO:0006457|protein folding |-14.3;R-HSA-3371556|Cellular response to heat stress|-13.8;
SN5	GO:0000079|regulation of cyclin-dependent protein serine/threonine kinase activity |-9.0;
SN6	GO:0002478|antigen processing and presentation of exogenous peptide antigen |-14.6;
SN7	R-HSA-379716|Cytosolic tRNA aminoacylation |-11.3;
SN8	GO:0036003|positive regulation of transcription from RNA polymerase II promoter in response to stress| -11.8
SN11	WP455|GPCRs, class A rhodopsin-like|-6.2;R-HSA-418594|G alpha (i) signalling events |-5.9;

Figure 5. DI abrogates TLR activation and promotes NRF2-mediated stress response. We adopted the PRE-CpG (green) schedule to specifically evaluate the effects of 100 μM DI on transcriptome of purified CLL cells. We performed RNAseq on $n = 6$ donors of primary CLL samples treated or not with 100 μM DI ON followed by the addition of 2.5 μg/mL CpG. For each paired contrast ("DI treated vs. ctrl", "CpG stimulated vs. ctrl", "DI+CpG treated and stimulated vs. ctrl" and "DI+CpG treated and stimulated versus CpG") we calculated the DEGs, as genes with $|\log_2 fc|>1$ and nominal p-value < 0.001 [41] and with those lists we performed enrichment and PPI analysis with Metascape [13]. (A) Circos plot showing the DEGs overlapping among the up- and downregulated lists of genes, (B) Heatmap showing the top 50 DEGs identified in the meta-analysis. (C) PPI network showing the connection among the genes in all the lists of DEGs: the colors in the circle of each gene represent their respective list. Subnetworks (SN) were used to identify closely connected neighborhoods. For each SN an enrichment analysis was performed with Metascape, and the most representative enrichment terms are reported).

metabolic activation and to a lesser extent was proapoptotic. DI reduced CpG-mediated metabolic activation and cytoprotection even when added after robust *in vitro* TLR stimulation. Surprisingly, DI reduced ATP basal levels when cells were incubated *ex-vivo* without CpG. This may indicate the memory of previous *in vivo* TLR stimulation without excluding the possibility of additional targets of DI activity.

Though one of the goals of our work was to study the effects of DI on purified leukemic cells where indeed the treatment promoted cell death, we also showed that the presence of normal

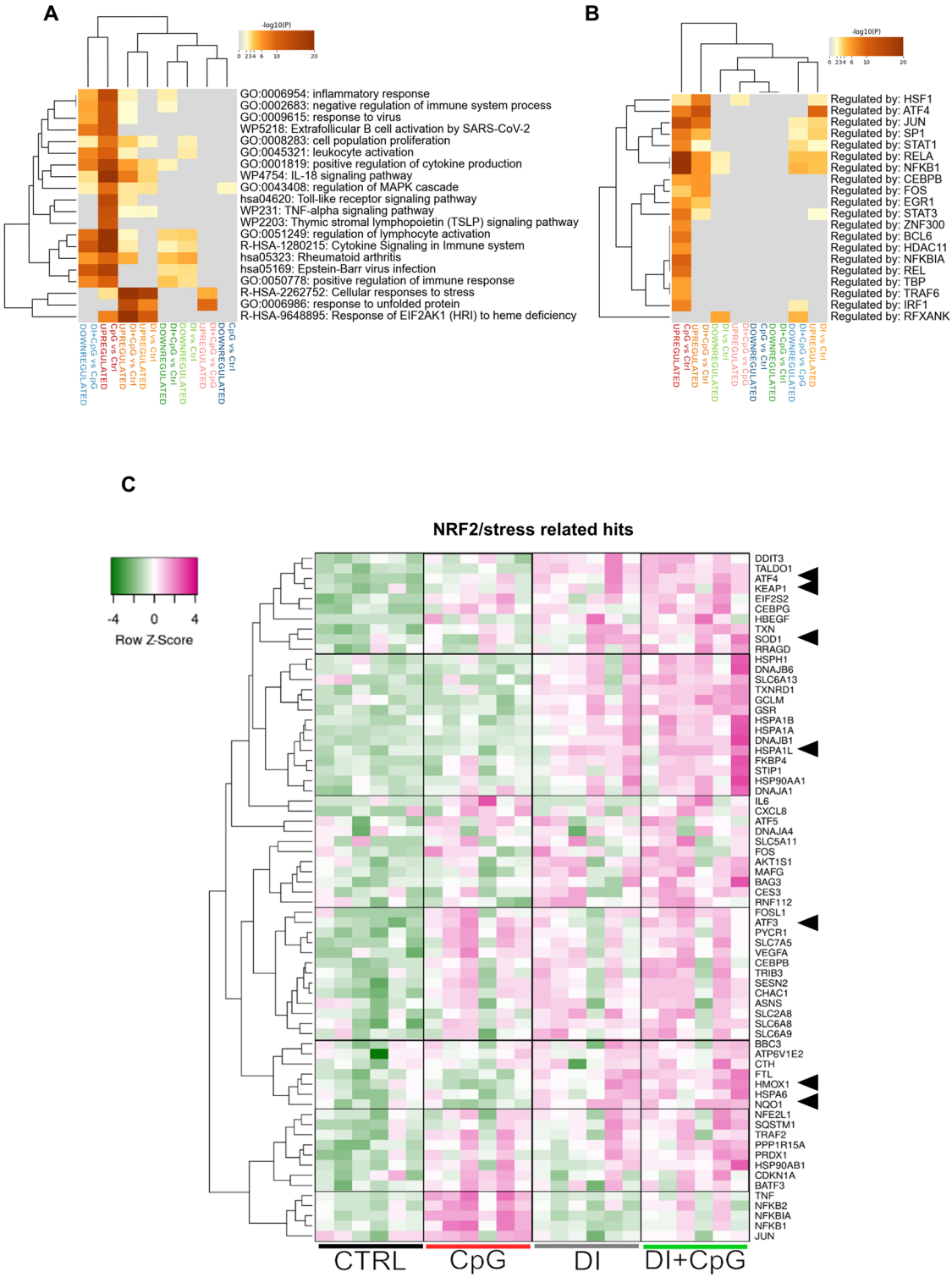

Figure 6. DI promotes stress-related pathways in CLL cells. The RNAseq data generated on $n = 6$ donors of primary CLL samples of Fig. 5 were further analyzed with Metascape (A) Heatmap showing the top 20 enriched terms among the lists of DEGs identified in the meta-analysis; (B) Enrichment analysis against TRRUST collection was performed and the Heatmap shows the enriched terms among the lists of DEGs identified in the meta-analysis; (C) Among the DI-specific enriched pathways emerged, we extracted those related to stress/NRF2. Following, we extracted the list of genes that hit the enriched pathways, and we created the Heatmap with log_2RPKM values.

leukocytes was not able to protect from the apoptotic effect of DI against CLL cells as it occurs in the case of other drugs when utilized *ex vivo* in co-culture systems [19].

It is also relevant to note that when DI was utilized on PBMC isolated from healthy donors, no relevant toxicities were apparent including on normal B cells. Notably, healthy B-lymphocytes are responsive to CpG in terms of IκBζ expression although at lower levels as compared with IκBζ-high CLL cases; in contrast, NF-κB p65 (which IκBζ is a cofactor of) is constitutively activated in CLL but not in normal B cells. That left only one possibility to explain this rather specific anti-leukemic effect, that is, DI appears to target a specific vulnerability of leukemic cells.

At a molecular level, our results show that in CLL cells DI did not induce ATF3 protein but, on the contrary, blocked TLR-mediated ATF3 induction thus supporting an ATF3-independent effect. In addition, our RNA-sequencing data show the induction of a signature related to electrophilic stress. Moreover, we observed induction of NQO1 in leukemic cells when incubated with DI suggesting that NQO1 may mediate, at least in part, DI function in a manner similar to what was previously observed in macrophages [16, 29]. Overall, our data support a bivalent role of DI in CLL cells where it can block inflammation by interrupting the secondary wave controlled by IκBζ, while at the same time inducing NRF2 signaling.

Although the NRF2 pathway is considered mainly a protective response that cancer cells may adapt to survive in challenging conditions [30], our data suggest that the opposite can happen where DI acts as an anti-tumor agent that at the same time induces NRF2 signaling. Interestingly. It was recently proposed that NRF2 may have a dual protumorigenic versus antitumorigenic role depending on the tumor stage and context, and NRF2 activation may lead to metabolic vulnerabilities [31]. Our data are in line with previous observations of increased NRF2 levels in CLL cells with respect to normal PBMC and their increased sensitivity to electrophilic compounds [21].

Finally, our transcriptomic analysis highlighted a DI-specific downregulation of several MHC class II genes. To note, a recent report demonstrated that B-cell receptor signaling can upregulate antigen presentation machinery including MHC class II genes [32]. This effect of DI may impact the activity of T-helper cells *in vivo* which are known to play a role in sustaining leukemic cells [33–35].

In conclusion, our data suggest that DI can have a dual role in inducing electrophilic stress independent from CpG and at the same time inhibiting the inflammatory and cytoprotective effect mediated by the TLR9/IκBζ axis. This effect is more evident in IκBζ-high samples as they are characterized by enhanced reactivity to microenvironmental stimuli (see Fig. S10 for a schematic representation).

Our correlative analyses on one side support the link between TLR-mediated inflammation, IκBζ overexpression, and DI immunomodulatory role, on the other side highlight the existence of novel unexpected mechanisms independent from classic TLR signaling that may uncover novel CLL vulnerabilities.

Materials and methods

Reagents

Class B CpG oligonucleotides specific for Human TLR9 (CpG ODN2006) and murine TLR9 (CpG ODN1826) were purchased from Invivogen and were used at a concentration of 2.5 μg/mL. LPS ultrapure O111:B4 (Invitrogen) was used at a concentration of 1 μg/mL. DI was purchased from Santa Cruz Biotechnology (sc-239775), dissolved in RPMI, and used at increasing concentrations from 50 to 200 μM as previously described [16].

Cells

Patients with CLL untreated or off therapy for more than 6 months were diagnosed according to the iwCLL Guidelines [36]; clinical and biological characteristics of the patients are reported in Tables S1 and S2. Peripheral blood (PB) samples were obtained after informed consent as part of a study approved by the institutional ethics committee (IRB code VIVI-CLL). We analyzed a total of 40 randomly selected patients' samples for the different analyses, and we measured the expression of IκBζ protein before and after 24 h CpG treatment in 38 of them.

Total PB mononuclear cells (PBMC) were isolated by Ficoll centrifugation from heparinized PB from healthy donors (IRB code Leu-Buffy_Coat) and patients with CLL (Lymphoprep; Axis-Shield Diagnostics, Dundee, UK); in addition, CLL and normal B cells were negatively selected using a B-cell enrichment kit (RosetteSep; StemCell Technologies). The purity of the isolated B cells was always greater than 95%. Splenocytes were isolated from TCL1-leukemic mice when the percentage of leukemic cells circulating in the PB exceeded 80%.

Cell viability and metabolic activation

Viable cells were counted using the automatic cell counter TC20 (Bio-Rad) after staining with trypan blue dye (Bio-Rad). ATP quantification was assessed using Cell Titer-Glo assay (Promega) and luminescence was measured using a Mithras LB 940 multimode microplate reader (Berthold Technologies).

Real-time PCR quantification

RNA was extracted and analyzed as previously described [11] using the following probes with CFX connect (Bio-Rad): Probe NFKBIZ (qHsaCEP0052487, Bio-Rad); Probe IL6 (Hs00985639m1, Thermo Fisher Scientific); Probe IL10 (Hs00961622_m1, Thermo Fisher Scientific); Probe Actin (qHsaCEP0036280, Bio-Rad); Probe 18s (qHsaCEP0049956, Bio-Rad); Probe NQO1 (qHsaCEP0039593, Bio-Rad); Probe TBP (qHsaCIP0036255, Bio-Rad).

RNA sequencing

RNA-seq data and methods have been deposited in NCBI's Gene Expression Omnibus[37] and are accessible through GSE226904 and GSE210972.

Heatmap were created with Heatmapper [38] with Log_2RPKM values.

Gene Ontology (GO), Kyoto Encyclopedia of Genes and Genomes, and BioCarta enrichment analysis were performed on the lists of DEGs using the Metascape platform [13]. The PPI networks were constructed with Metascape and modified with Cytoscape 3.9.1 platform [39]. Venn diagrams were created with InteractiVenn [40].

Western blotting

Cell lysates were prepared and analyzed as previously described with the following antibodies: NFKBIZ (Cell Signaling Technology, #9244, 1:1000); NFKBIZ (Cell Signaling Technology, #93726, 1:1000); anti-β-Actin HRP-conjugated (Sigma 1:20000); Anti-ATF3 (Cell Signaling Technology, E9J4N #18665, 1:1000); Anti-PARP (Cell Signaling Technology, #9542, 1:1000); Anti-NQO1 (Sigma-Aldrich, HPA007308, 1:1000); Anti-Rabbit HRP-conjugated (Sigma-Aldrich, A0545, 1:4000); Anti-BCL-xL (Cell Signaling Technology, 54H6 #2764, 1:1000); Anti-Mcl1 (Cell Signaling Technology, D35A5 #5453, 1:1000); Anti-NF-κB p65 (Cell Signaling Technology, D14E12 #8242, 1:1000); Anti-phospho-NF-κB p65 (Ser536; Cell Signaling Technology, 93H1 #3033, 1:1000); Anti-NF-κB p50 (Cell Signaling Technology, D4P4D #13586, 1:1000).

Flow cytometry analysis

For all experiments data were acquired on a BD Navios flow cytometer (BD Pharmingen) and analyzed using FCS Express 7 Flow Cytometry software (De Novo Software). For the analysis of PBMC, cells were stained with viability dye 660 or viability dye 780 (e-Bioscience/Thermo Fisher Scientific) and following with antibodies against CD5-PC7, CD19-ECD, and CD16-PC5 (Beckman Coulter). To quantify IκBζ expression, cells were fixed and permeabilized with FIX/PERM kit (BD Pharmigen) and following stained with IκBζ-PE (hft2nap clone, e-Bioscience). For apoptotic cell quantification, cells were stained with Annexin V Apoptosis Detection Kits kit (e-Bioscience/Thermo Fisher Scientific) following the manufacturer's protocol.

Statistical analysis

Statistical analyses were performed with Prism Software (GraphPad Prism 9 Software) and the details of each analysis are described in the corresponding figure legend. $p \leq 0.05$ was considered significant.

Acknowledgements: The research leading to these results has received funding from AIRC under IG-2019 -ID. 23088 project—PI Marta Muzio. This work was supported in part by Ministero della Salute under Ricerca Finalizzata 2018 -ID. RF-2018-12367072 project—PI Muzio Marta and Ricerca Finalizzata 2018 -ID. RF-2018–12368231 project: PI Paolo Ghia; AIRC under 5 per Mille 2018 -ID. 21198 program—PI Foà Roberto, G.L. PG, and under Investigator Grant #20246 - P.I. PG; ERA NET TRANSCAN-2 Joint Transnational Call for Proposals: JTC 2016 (project #179 NOVEL), project code (MIS) 5041673 (to PG).
Open access funding provided by BIBLIOSAN.

Conflict of interest: LS received honoraria from AbbVie, AstraZeneca, and Janssen. PG received honoraria from AbbVie, AstraZeneca, ArQule/MSD, Celgene/Juno/BMS, Janssen, Lilly/loxo, Roche; Research support from AbbVie, AstraZeneca, Janssen. The remaining authors declare no conflict of interest.

Author Contributions: Ilenia Sana designed experiments, performed research, analyzed the data, and wrote the manuscript; Maria Elena Mantione performed experiments and analyzed the data; Miriam Meloni performed experiments and analyzed the data; Michela Riba performed RNA seq analysis and analyzed data; Pamela Ranghetti prepared and analyzed patient samples; Lydia Scarfò provided patient samples and clinical information and analyzed the data; Paolo Ghia supervised patient samples and clinical data collection and analysis, analyzed the data and edited the manuscript; Marta Muzio designed and supervised the study, analyzed the data, and wrote the manuscript.

Data availability statement: The RNAseq data that support the findings of this study are openly available in Gene Expression Omnibus at [https://www.ncbi.nlm.nih.gov/geo/], reference number GSE226904 and GSE210972. The other data that support the findings of this study are available from the corresponding author upon reasonable request.

Peer review: The peer review history for this article is available at https://publons.com/publon/10.1002/eji.202350418

References

1 **Bosch, F. and Dalla-Favera, R.**, Chronic lymphocytic leukaemia: from genetics to treatment. *Nat. Rev. Clin. Oncol.* 2019. **16**: 684–701.

2 **Dadashian, E. L., McAuley, E. M., Liu, D., Shaffer, A. L., Young, R. M., Iyer, J. R., Kruhlak, M. J. et al.**, TLR signaling is activated in lymph node–resident CLL cells and is only partially inhibited by ibrutinib. *Cancer Res.* 2019. **79**: 360–371.

3 **Bruch, P.-M., Giles, H. A., Kolb, C., Herbst, S. A., Becirovic, T., Roider, T., Lu, J. et al.**, Drug-microenvironment perturbations reveal resistance mechanisms and prognostic subgroups in CLL. *Mol. Syst. Biol.* 2022. **18**: e10855.

4 **Longo, P. G., Laurenti, L., Gobessi, S., Petlickovski, A., Pelosi, M., Chiusolo, P., Sica, S. et al.**, The Akt signaling pathway determines the different proliferative capacity of chronic lymphocytic leukemia B-cells from patients with progressive and stable disease. *Leukemia* 2007. **21**: 110–120.

5 **Kennedy, E., Coulter, E., Halliwell, E., Profitos-Peleja, N., Walsby, E., Clark, B., Phillips, E. H. et al.**, TLR9 expression in chronic lymphocytic leukemia identifies a promigratory subpopulation and novel therapeutic target. *Blood* 2021, **137**: 3064–3078.

6 **Tarnani, M., Laurenti, L., Longo, P. G., Piccirillo, N., Gobessi, S., Mannocci, A., Marietti, S. et al.**, The proliferative response to CpG-ODN stimulation predicts PFS, TTT and OS in patients with chronic lymphocytic leukemia. *Leuk. Res.* 2010. **34**: 1189–1194.

7 **Dampmann, M., Görgens, A., Möllmann, M., Murke, F., Dührsen, U., Giebel, B. and Dürig, J.**, CpG stimulation of chronic lymphocytic leukemia cells induces a polarized cell shape and promotes migration in vitro and in vivo. *PLoS One* 2020. **15**: e0228674.

8 **Efremov, D. G., Bomben, R., Gobessi, S. and Gattei, V.**, TLR9 signaling defines distinct prognostic subsets in CLL. *Front. Biosci.* 2013. **18**: 371.

9 **Bomben, R., Gobessi, S., Dal Bo, M., Volinia, S., Marconi, D., Tissino, E., Benedetti, D. et al.**, The miR-1792 family regulates the response to toll-like receptor 9 triggering of CLL cells with unmutated IGHV genes. *Leukemia* 2012. **26**: 1584–1593.

10 **Fonte, E., Apollonio, B., Scarfò, L., Ranghetti, P., Fazi, C., Ghia, P., Caligaris-Cappio, F. et al.**, In vitro sensitivity of CLL cells to fludarabine may be modulated by the stimulation of toll-like receptors. *Clin. Cancer Res.* 2013. **19**: 367–379.

11 **Fonte, E., Vilia, M. G., Reverberi, D., Sana, I., Scarfò, L., Ranghetti, P., Orfanelli, U. et al.**, Toll-like receptor 9 stimulation can induce IκBζ expression and IgM secretion in chronic lymphocytic leukemia cells. *Haematologica* 2017. **102**: 1901–1912.

12 **Willems, M., Dubois, N., Musumeci, L., Bours, V. and Robe, P. A.**, IκBζ: an emerging player in cancer. *Onco. Targets Ther.* 2016. **4**: 66310–66322.

13 **Zhou, Y., Zhou, B., Pache, L., Chang, M., Khodabakhshi, A. H., Tanaseichuk, O., Benner, C. et al.**, Metascape provides a biologist-oriented resource for the analysis of systems-level datasets. *Nat. Commun.* 2019. **10**: 1523.

14 **Zhou, G. and Xia, J.**, OmicsNet: A web-based tool for creation and visual analysis of biological networks in 3D space. *Nucleic Acids Res.* 2018. **46**: W514–W522.

15 **Galicia-Vázquez, G. and Aloyz, R.**, Metabolic rewiring beyond Warburg in chronic lymphocytic leukemia: How much do we actually know? *Crit. Rev. Oncol. Hematol.* 2019. **134**: 65–70.

16 **Bambouskova, M., Gorvel, L., Lampropoulou, V., Sergushichev, A., Loginicheva, E., Johnson, K., Korenfeld, D. et al.**, Electrophilic properties of itaconate and derivatives regulate the IκBζ-ATF3 inflammatory axis. *Nature* 2018. **556**: 501–504.

17 **Mills, E. L., Ryan, D. G., Prag, H. A., Dikovskaya, D., Menon, D., Zaslona, Z., Jedrychowski, M. P. et al.**, Itaconate is an anti-inflammatory metabolite that activates Nrf2 via alkylation of KEAP1. *Nature* 2018. **556**: 113–117.

18 **O'Neill, L. and Artyomov, M. N.**, Itaconate: the poster child of metabolic reprogramming in macrophage function. *Nat. Rev. Immunol.* 2019. **19**: 273–281.

19 **Primo, D., Scarfò, L., Xochelli, A., Mattsson, M., Ranghetti, P., Espinosa, A. B., Robles, A. et al.**, A novel ex vivo high-throughput assay reveals antiproliferative effects of idelalisib and ibrutinib in chronic lymphocytic leukemia. *Onco. Targets Ther.* 2018. **9**: 26019–26031.

20 **Bichi, R., Shinton, S. A., Martin, E. S., Koval, A., Calin, G. A., Cesari, R., Russo, G. et al.**, Human chronic lymphocytic leukemia modeled in mouse by targeted TCL1 expression. *Proc. Natl. Acad. Sci. USA* 2002. **99**: 6955–6960.

21 **Wu, R. P., Hayashi, T., Cottam, H. B., Jin, G., Yao, S., Wu, C. C. N., Rosenbach, M. D. et al.**, Nrf2 responses and the therapeutic selectivity of electrophilic compounds in chronic lymphocytic leukemia. *Proc. Natl. Acad. Sci. USA* 2010. **107**: 7479–7484.

22 **Nakkala, J. R., Yao, Y., Zhai, Z., Duan, Y., Zhang, D., Mao, Z., Lu, L. et al.**, Dimethyl itaconate-loaded nanofibers rewrite macrophage polarization, reduce inflammation, and enhance repair of myocardic infarction. *Small* 2021. **17**: 2006992.

23 **Shan, Q., Li, X., Zheng, M., Lin, X., Lu, G., Su, D. and Lu, X.**, Protective effects of dimethyl itaconate in mice acute cardiotoxicity induced by doxorubicin. *Biochem. Biophys. Res. Commun.* 2019. **517**: 538–544.

24 **Kuo, P.-C., Weng, W.-T., Scofield, B. A., Paraiso, H. C., Brown, D. A., Wang, P.-Y., Yu, I.-C. et al.**, Dimethyl itaconate, an itaconate derivative, exhibits immunomodulatory effects on neuroinflammation in experimental autoimmune encephalomyelitis. *J. Neuroinflammation*. 2020. **17**: 138.

25 **Gu, L., Lin, J., Wang, Q., Li, C., Peng, X., Fan, Y., Lu, C. et al.**, Dimethyl itaconate protects against fungal keratitis by activating the Nrf2/HO-1 signaling pathway. *Immunol. Cell Biol.* 2020. **98**: 229–241.

26 **Gautam, A. K., Kumar, P., Raj, R., Kumar, D., Bhattacharya, B., Rajinikanth, P. S., Chidambaram, K. et al.**, Preclinical evaluation of dimethyl itaconate against hepatocellular carcinoma via activation of the e/iNOS-mediated NF-κB-dependent apoptotic pathway. *Front. Pharmacol.* 2021. **12**: 823285.

27 **Wang, Q., Li, X. L., Mei, Y., Ye, J.-C., Fan, W., Cheng, G.-H., Zeng, M.-S. et al.**, The anti-inflammatory drug dimethyl itaconate protects against colitis-associated colorectal cancer. *J. Mol. Med.* 2020. **98**: 1457–1466.

28 **Hayashi, K., Nakazato, Y., Ouchi, M., Fujita, T., Endou, H. and Chida, M.**, Antitumor effect of dimethyl itaconate on thymic carcinoma by targeting LDHA-mTOR axis. *Life Sci.* 2021. **282**: 119847.

29 **Kimura, A., Kitajima, M., Nishida, K., Serada, S., Fujimoto, M., Naka, T., Fujii-Kuriyama, Y. et al.**, NQO1 inhibits the TLR-dependent production of selective cytokines by promoting IκB-ζ degradation. *J. Exp. Med.* 2018. **215**: 2197–2209.

30 **Sanchez-Lopez, E., Ghia, E. M., Antonucci, L., Sharma, N., Rassenti, L. Z., Xu, J., Sun, B. et al.**, NF-κB-p62-NRF2 survival signaling is associated with high ROR1 expression in chronic lymphocytic leukemia. *Cell Death Differ.* 2020. **27**: 2206–2216.

31 **Pillai, R., Hayashi, M., Zavitsanou, A.-M. and Papagiannakopoulos, T.**, NRF2: KEAPing tumors protected. *Cancer Discov.* 2022. **12**: 625–643.

32 **Minton, A. R., Smith, L. D., Bryant, D. J., Strefford, J. C., Forconi, F., Stevenson, F. K., Tumbarello, D. A. et al.**, B-cell receptor dependent phagocytosis and presentation of particulate antigen by chronic lymphocytic leukemia cells. *Explor. Target Antitumor Ther.* 2022. **3**: 37–49.

33 **Grioni, M., Brevi, A., Cattaneo, E., Rovida, A., Bordini, J., Bertilaccio, M. T. S., Ponzoni, M. et al.**, CD4+ T cells sustain aggressive chronic lymphocytic leukemia in Eμ-TCL1 mice through a CD40L-independent mechanism. *Blood Adv.* 2021. **5**: 2817–2828.

34 **Bagnara, D., Kaufman, M. S., Calissano, C., Marsilio, S., Patten, P. E. M., Simone, R., Chum, P. et al.**, A novel adoptive transfer model of chronic lymphocytic leukemia suggests a key role for T lymphocytes in the disease. *Blood* 2011. **117**: 5463–5472.

35 **Os, A., Bürgler, S., Ribes, A. P., Funderud, A., Wang, D., Thompson, K. M., Tjønnfjord, G. E. et al.**, Chronic lymphocytic leukemia cells are activated and proliferate in response to specific T helper cells. *Cell Rep.* 2013. **4**: 566–577.

36 **Hallek, M., Cheson, B. D., Catovsky, D., Caligaris-Cappio, F., Dighiero, G., Döhner, H., Hillmen, P. et al.**, iwCLL guidelines for diagnosis, indications

for treatment, response assessment, and supportive management of CLL. *Blood* 2018. **131**: 2745–2760.

37 **Edgar, R.**, Gene Expression Omnibus: NCBI gene expression and hybridization array data repository. *Nucleic Acids Res.* 2002. **30**: 207–210.

38 **Babicki, S.**, **Arndt, D.**, **Marcu, A.**, **Liang, Y.**, **Grant, J. R.**, **Maciejewski, A. and Wishart, D. S.**, Heatmapper: web-enabled heat mapping for all. *Nucleic Acids Res.* 2016. **44**: W147–W153.

39 **Excoffier, L.**, **Gouy, A.**, **Daub, J. T.**, **Shannon, P.**, **Markiel, A.**, **Ozier, O.**, **Baliga, N. S. et al.**, Cytoscape: a software environment for integrated models of biomolecular interaction networks. *Nucleic. Acids Res.* 2017. **45**: e149.

40 **Heberle, H.**, **Meirelles, V. G.**, **da Silva, F. R.**, **Telles, G. P. and Minghim, R.**, InteractiVenn: a web-based tool for the analysis of sets through Venn diagrams. *BMC Bioinf.* 2015. **16**: 169.

41 **Xu, J.**, **Gong, B.**, **Wu, L.**, **Thakkar, S.**, **Hong, H. and Tong, W.**, Comprehensive assessments of RNA-seq by the SEQC consortium: FDA-led efforts advance precision medicine. *Pharmaceutics* 2016. **8**: 8.

Abbreviations: **CLL**: chronic lymphocytic leukemia · **DEGs**: differentially expressed genes · **DI**: dimethyl itaconate · **PB**: peripheral blood · **PBMC**: peripheral blood mononuclear cells · **PPI**: protein–protein interaction · **TLR**: toll-like receptor

Full correspondence: Dr. Marta Muzio, Cell Signaling Unit, Division of Experimental Oncology, IRCCS San Raffaele Scientific Institute, San Raffaele Hospital, via Olgettina 58, Milano 20132, Italy
e-mail: muzio.marta@hsr.it

Received: 4/2/2023
Revised: 30/6/2023
Accepted: 7/8/2023
Accepted article online: 10/8/2023